Original Research

Investigating the Stimulus-Dependent Temporal Dynamics of the BOLD Signal Using Spectral Methods

Karsten Müller, PhD,* Toralf Mildner, PhD, Gabriele Lohmann, PhD, and D. Yves von Cramon, MD

Purpose: To compare several spectral parameters using different durations of visual hemifield stimulation in order to explore the different temporal behavior of the blood oxygenation-level dependent (BOLD) signal in various brain regions.

Materials and Methods: Spectral methods were applied to three different groups of subjects with visual stimulation lasting 6, 12, and 30 seconds. Furthermore, diffusion weighting was applied in an interleaved way. The core of the data processing was the computation of the spectral density matrix using the multidimensional weighted covariance estimate. Spectral parameters of coherence and phase shift were computed.

Results: The correlation between signal changes and phase shifts was dependent on the duration of the visual stimulation. The shorter the duration of visual stimulation, the stronger the correlation between percentage signal change and phase shift.

Conclusion: The experiments with short and long stimuli differed mainly in the distribution of the activated voxels in the plane of percentage signal change and phase shift. It was revealed that the height of the signal change depends on the phase shift, whereas the diffusion weighting has no influence.

Key Words: functional magnetic resonance imaging; fMRI; diffusion weighting; spectral analysis; coherence; phase shift
J. Magn. Reson. Imaging 2003;17:375–382.

THE AIM OF THIS STUDY was to investigate the stimulus-dependent temporal dynamics of the blood oxygenation-level dependent (BOLD) response function in the human brain.

Max Planck Institute of Cognitive Neuroscience, Leipzig, Germany.
*Address reprint requests to: K. M., Max Planck Institute of Cognitive Neuroscience, Stephanstrasse 1a, D-04103 Leipzig, Germany. E-mail: karstenm@cns.mpg.de
Received March 21, 2002; Accepted October 23, 2002
DOI 10.1002/jmri.10268
Published online in Wiley InterScience (www.interscience.wiley.com).

Recent studies investigating the BOLD response function in the spectral domain employed long blocks of visual stimuli(1,2). In the current work, spectral methods are applied to functional magnetic resonance imaging (fMRI) data using different durations of visual hemifield stimulation. Several spectral parameters are compared. Our analysis reveals differences in the distribution of the phase shifts of activated voxels.

There is still much controversy concerning the reasons for the varying temporal behavior of the BOLD signal in different brain regions (3–7). Using the general linear model, Miezin et al (3) investigated the relative timing of the BOLD signal in different cerebral regions within the same subject. Their results showed only a rough temporal relation between the BOLD signal in different brain regions. The authors pointed to differences in the vasculature as the reason for the inability to reliably predict BOLD response in different cerebral regions.

A further study by Menon et al (4) also sought to explore temporal variations in the onset of the BOLD response in different brain regions. The authors discussed various features of the fMRI signal that can be used to describe the varying temporal behavior of the BOLD response. From their data, robust timing information among activated brain regions could be retrieved which corresponded exactly to the stimulus presentation timing, even across hemispheres. However, there are several possible explanations for the variation in the observed delays. Because the observed BOLD contrast is sensitive to the vessel diameter (5), different delays could be due to differences in the underlying vasculature across regions. Specifically, delays could be brought on by larger-scale veins. However, Rosen et al(6) observed the longest delays even in regions where the vasculature is minimal. Therefore, it was concluded that additional factors may influence the delay of the BOLD signal (6,7).

The MR signal can be considered to consist of an extravascular and an intravascular contribution (8,9). The intravascular signal contribution associated with postcapillary vessels can be suppressed using diffusion weighting, because the signal of flowing spins is dephased (10). This can be achieved by inserting a bi-

polar gradient pair before the readout of the echo-planar image. In this study, we applied the diffusion weighting in an interleaved manner, i.e., only on alternate echo-planar imaging (EPI) scans. This allowed a better comparison of the BOLD signal with and without diffusion weighting, since the method does not suffer from the intertrial variability of the BOLD signal (11).

Maps of coherence and phase shift were generated from both the diffusion- and nondiffusion-weighted EPI time series using spectral analysis methods as described in 2. A brief introduction into the theory is given in the following section. The method provides information about the temporal dynamics of the BOLD response function. The core of the method is the estimation of the cross-covariance function and the spectral density matrix.

The sample coherence measure can be interpreted as a measure of the degree of linear association of the time series. Therefore, brain regions with a high coherence value can be considered as areas that belong to the same network structure. Because of the different relative timing of the onset of the BOLD response in different brain regions (4), phase shifts can be used to investigate the temporal behavior of the hemodynamic response.

MATERIALS AND METHODS

Spectral Theory

In this section, we introduce the spectral parameters that are used in this work. The theory of spectral analysis was previously successfully applied to fMRI data (1,2). For a detailed treatment see the monographs of Hannan (12) and Priestley (13).

Real, time-varying physical processes require more than one measurement to give a description of their behavior. Thus, the fMRI process at each time point is represented by a set of time-dependent measurements $\mathbf{X}(t) = X_1(t), \ldots, X_N(t)$. Suppose this vector contains stochastic processes in the same probability space. Furthermore, let us assume that the mean values are constant in time and the covariances depend upon the time displacement, and not on the time point itself, i.e.,

$$E[X_j(\tau + t)X_k(t)] = E[X_j(\tau)X_k(0)] = C_{jk}(\tau) \qquad (1)$$

where X_j and X_k are arbitrary elements of the vector $\mathbf{X}$. The function $C_{jk}(\tau)$ is called the cross-covariance function of the stochastic processes X_j and X_k. The covariances depend on τ, the lag between the time arguments, but not on t. Although the autocovariances $C_{jj}(\tau)$ are even functions, the cross-covariance functions are not. This has an important effect on the spectral representation of the cross-covariances. There exists a unique nonnegative definite measure F_{jk} such that

$$C_{jk}(\tau) = \int e^{i\lambda\tau} dF_{jk}(\lambda) \qquad (2)$$

Equation [2] is the well-known spectral representation, and the measure F_{jk} is called the cross-spectral distribution of the stochastic processes X_j and X_k (see, e.g., 13). The measure λ is the angular frequency measured in radians per unit time. Since the cross-covariance function is not even, the cross-spectral distribution is a complex value with a nonvanishing imaginary part. The measure F_{jk} describes the relationship between the two time series X_j and X_k that belong to the multidimensional stochastic process. The derivative of this function is called the cross-spectral density function

$$f_{jk}(\lambda) = \frac{dF_{jk}(\lambda)}{d\lambda} \qquad (3)$$

which is the basic second-order parameter for our further considerations. This function can be interpreted as a measure of covariance between the respective frequency components in the two time series.

In the following, we are interested in the relation between pairs of time series $X_j(t)$ and $X_k(t)$ of the multivariate stochastic process. The interrelation can be described via the bivariate spectral densities. These parameters are also called bivariate spectral parameters. The polar representation

$$f_{jk}(\lambda) = |f_{jk}(\lambda)| e^{i\vartheta_{jk(\lambda)}} \qquad (4)$$

of the spectral density function further gives a set of bivariate spectral parameters that play a central role in this study. The function $\vartheta_{jk}(\lambda)$ is called the phase shift of $X_j(t)$ over $X_k(t)$, and is commonly interpreted as the average phase shift of two time series at frequency λ. The phase shift can also be converted to time lag by dividing by the frequency λ. Thus the parameter of time lag between two time series can be computed at various frequencies of interest. The function

$$\rho_{jk}(\lambda) = \frac{|f_{jk}(\lambda)|}{(f_{jj}(\lambda) f_{kk}(\lambda))^{1/2}} \qquad (5)$$

is called coherence (or coefficient of coherence) and is a crucial parameter for measuring relationships between time series. It is a measure for the degree of linear association between two time series and can be interpreted quantitatively. In principle, the coherence can be referred to as a generalization of the correlation coefficient in the frequency domain. The extreme values, zero and one, correspond to the complete lack of correlation and the maximal degree of correlation possible for a definition of correlation that makes sense in the time-series context.

In the following, we give an introduction to how an estimation of spectral parameters is obtained. Certain characteristics of random variables are estimated using a sample that can be considered a realization of the hidden phenomenon. Usually the sample is a set of realizations of a stochastic process for a small subset of time points only. However, if the observations are interpreted as realizations of a random process, there is often only one realization with many timesteps. In this case, the characteristics of the random variables are estimated by averaging over time and not over realiza-

tions. Let $\mathbf{X}(t)$ be a realization of a multidimensional stochastic process. Without loss of generality, let us assume that $\mathbf{X}(t)$ is already zero-mean. Then the function

$$\hat{C}_{N,\,jk}(s) = \begin{cases} \dfrac{1}{N}\displaystyle\sum_{t=1}^{N-s} X_j(s+t)X_k(t), & s = 0,1,\ldots,N-1 \\ \hat{C}_{N,kj}(-s), & s = -1,\ldots,-N+1 \end{cases} \tag{6}$$

is called the multidimensional weighted covariance estimate based on the realization $\mathbf{X}(t)$. For $|s| \geq N$, the estimation for the cross-covariance is zero. A naive way to estimate the spectral density would be to compute the discrete Fourier transform of the multidimensional weighted covariance estimate, which is also called the periodogram matrix.

Although the covariance estimate converges to the covariance, its discrete Fourier transform does not converge to the spectral density. Therefore, in general, the periodogram is not an appropriate estimation for the spectral density (12). The problem is that in the neighborhood of N, only a small set of observations is used to estimate the covariance function. In the worst case, only one element of the time course is used. Such an estimation is not admissible. Therefore, a number $M_N < N$ is chosen in order to determine how many elements of the covariance estimation are used to estimate the spectral density. This number M_N is called the maximal displacement or spectral window size. The estimation of f has the form

$$\hat{f}_{N,jk}(\lambda) = \frac{1}{2\pi}\sum_{s=-M_N}^{M_N} e^{-i\lambda s}\omega\left(\frac{s}{M_N}\right)\hat{C}_{N,\,jk}(s) \tag{7}$$

where the function ω is called a lag window generator. Such a weighting function is used because the periodogram has variance that does not approach zero with increasing N. The lag window generator ω is a real, even and bounded function which is defined on the interval $[-1, 1]$. There are many kinds of such functions. For our calculations, we use the Parzen lag window generator, which is very convenient for computing the spectral density estimate. See 13 for a discussion of various lag window generators.

Using the estimation in Eq. [7], one can give an estimation of the coefficient of coherence and phase shift inserting the spectral density estimate in Eq. [4] and [5]. In this study, we compute the sample coherence and give an estimation for the phase angle for different fMRI time series. Because we are also interested in the distribution of the estimated parameters, confidence intervals (14) for the obtained estimations can be computed. For a detailed treatment, see also Hannan's excellent monograph (13).

Stimuli and Imaging Procedure

Experiments were performed using a 3 T whole-body scanner (Bruker Medical, Ettlingen, Germany). A birdcage resonator of 28 cm i.d. was used for RF transmission and signal reception. Gradient performance was 45 mT/m switchable within 320 μs. For functional imaging a gradient-echo EPI sequence with a 64 × 64 acquisition matrix and a voxel size of 3 × 3 × 5 mm was used (acquisition bandwidth-100 kHz, echo train length-41 msec). The center of k-space was acquired at 25% of the echo train length. A flip angle of 45° for RF excitation and a repetition time (TR) of 500 msec were used. The echo time (TE) was set to 48 msec. Diffusion weighting was added by inserting a bipolar gradient pair applied simultaneously along the xyz-axes with a spacing between the onset of the bipolar gradients of Δ = 20 ms and a duration of δ = 15 ms. The gradient strength was set to give a b-value of 50 seconds mm^{-2}. A b-value of 50 seconds mm^{-2} results in a vascular signal loss of more than 75% (15).

In the same plane as the functional images, conventional anatomical images were acquired using a T1-weighted Modified Driven-Equilibrium Fourier Transform (MDEFT) (16) sequence (TE = 10 msec, TR = 1300 msec, 256 × 256 matrix). These images were obtained with a non-slice-selective inversion pulse followed by a single excitation of each slice (17).

A total of eight subjects (three males and five females), mean age-25 years participated in the experiment. All were right-handed and had normal or corrected-to-normal vision. All subjects provided informed consent prior to the scanning session. The subjects was on the scanner bed, and cushions were used to reduce head motion. Stimuli were projected by an LCD projector onto a back-projection screen mounted in the bore of the magnet behind the subject's head. Subjects viewed the screen wearing mirror glasses.

For task-induced activation a simple visual task was employed. During periods of control, subjects had to watch a small gray fixation-cross positioned in the center of a black screen. To focus their attention, the subjects had to press a button each time they saw a small black hole appear in the center of the fixation-cross at randomized time intervals. During periods of stimulation, a 7 × 5 array of red L-shapes randomly rotating at a frequency of 8 Hz on the black background was presented as a strong visual stimulus while the subjects had to perform the same search task as during the control periods.

The length of visual stimulation was not equal for all subjects. Subjects were partitioned into three groups with different durations of visual hemifield stimulation. For the first group of two subjects, stimuli lasted 30 seconds with control periods of 30 seconds. Five complete cycles of visual stimulation and control (a total of 600 EPI scans) were recorded. The second group of two subjects had stimuli with a duration of 12 seconds and control periods with a length of 78 seconds. Six complete cycles of visual stimulation and control (a total of 1080 EPI scans) were recorded. For the third group of four subjects, the stimuli lasted 6 seconds with control periods of 54 seconds. Six complete cycles of visual stimulation and control (a total of 720 EPI scans) were recorded. For all three groups, the control periods lasted at least 30 seconds to ensure that the BOLD signal returned to resting level (18).

For all subjects, three slices were acquired parallel to and centered in the primary visual cortex. One com-

plete dummy cycle, i.e. stimulation, RF pulses and gradient noise, was performed before data recording was commenced. Diffusion weighting was applied in an interleaved manner, i.e., every non-diffusion-weighted EPI scan was followed by a diffusion-weighted EPI scan.

Data Analysis

fMRI data were analyzed on an SGI Origin 2000 using spectral analysis tools implemented as described in the section on estimation of spectral parameters. The software was validated in a previous study (2) using synthetic data sets. For preprocessing, statistics, and visualization of the data, the software package Lipsia (19) was used.

First, slice acquisition time differences were corrected by sinc-interpolation. The mathematical background is the well-known Nyquist-Shannon sampling theorem, which shows that any continuous band-limited function is completely determined by discrete measurements taken at a constant sampling interval (20). Functional data were corrected for motion using a matching metric based on linear correlation. Baseline drifts were removed by temporal filtering, applying a high-pass filter using a discrete Fourier transform with a cutoff frequency of 1/120 Hz. Preprocessing was finalized by applying spatial filtering using a Gaussian kernel with a standard deviation (SD) of 0.8 pixels.

The statistical evaluation was based on least-squares estimation using the general linear model (21) for serially autocorrelated observations (22,23). The design matrix was generated using a boxcar (square wave) function and a response delay of 6 seconds. The model equation, including the observation data, the design matrix, and the error term, was convolved with a Gaussian kernel of dispersion of 4 seconds full width at half maximum (FWHM). The model includes an estimate of temporal autocorrelation that is used to estimate the effective degrees of freedom (23).

The main data processing task was the computation of the spectral density matrix using the multidimensional weighted covariance estimate. To select a reference voxel, we chose the maximum of the associated statistical parametric map. Computation was performed for each voxel of the image. The spectral density matrix was computed for the task frequency obtained by the power spectrum of the data. For all subjects, the Parzen lag window generator was used as the specific weight sequence. However, the properties of the spectral density estimate depend more critically on the choice of the spectral window size than on the form of the window, i.e., the lag window generator (13). We adjusted the spectral window size in order to get an optimal sampling rate for the data in the frequency domain with appropriate equivalent degrees of freedom > 50 (14). To compare the results between subjects, the size of the spectral window was set to 1/10 of the length of the timecourse. The resulting equivalent degree of freedom was 53.3 for all subjects.

Using the estimated spectral density matrix, the sample coherence matrix and the matrix of the phase shift estimation were computed. These matrices contain the bivariate sample coherence measure and the phase shift estimation of the time courses of the selected reference voxel with all voxels of the image. For visualization, maps of sample coherence and phase shift were generated that were overlaid on associated anatomical images. The maps of coherence were thresholded. Voxels with a coherence value of more than a threshold of 0.8 were used to visualize the phase shift. To validate the estimation of coherence and phase, confidence intervals were computed as described in 2 and 14. Also, maps of confidence intervals were generated for voxels with a coherence value of > 0.8, and for visualization these maps were overlaid on anatomical images.

We also computed maps of percentage signal changes of the BOLD signal. For each trial, the amplitude of the BOLD signal was computed by subtracting the rest amplitude from the peak amplitude of the signal, which were obtained by averaging neighboring time points near the end of the trial and at the maximum of the BOLD signal, respectively. For each voxel, percentage signal changes were finally averaged over all trials.

RESULTS

For all subjects, the data were processed as described in the previous section. Diffusion and non-diffusion-weighted functional images were evaluated separately. Because of the interleaved measurement technique, maps of diffusion and non-diffusion-weighted images could be compared. Maps of sample coherence show congruent regions in diffusion and non-diffusion-weighted data sets for all subjects. Striate and extrastriate visual cortices show a sample coherence above the selected threshold of 0.8. Because the coherence coefficient can be interpreted as a measure of the degree of linear association of time series, the map of coherence shows brain regions that belong to a network structure. In our experiment, visual cortical regions around the calcarine sulcus up to extrastriate visual areas belong to that network.

The maps of phase shift show voxels with positive and negative phase displacements in the primary visual cortex. Brain regions with an early response can be separated from areas with a late response. Figure 1 shows an example with a visual stimulation duration of 30 seconds, and Figure 2 shows phase maps with a visual stimulation duration of 6 seconds. These maps show BOLD phase shifts of about 1 and 2 seconds for the short and long stimulus, respectively. The dot plots of Figures 3 and 4 also show these phase shifts for the short and long stimulus. Moreover, the phase shifts of the BOLD signal can also be seen in the trial averages (see Fig. 1 and 2). The number of coherent voxels increases with the length of the stimulation (see bracketed numbers in the r_{ed} column of Table 1).

To evaluate the similarity between phase shifts in non-diffusion- and diffusion-weighted fMRI time series, the correlation was calculated within areas showing a sample coherence value above 0.8. We found a strong correlation above 0.8 for all subjects (see r_{ed} in Table 1). This correlation is independent of the duration of visual stimulation, and the selection of the spectral window size.

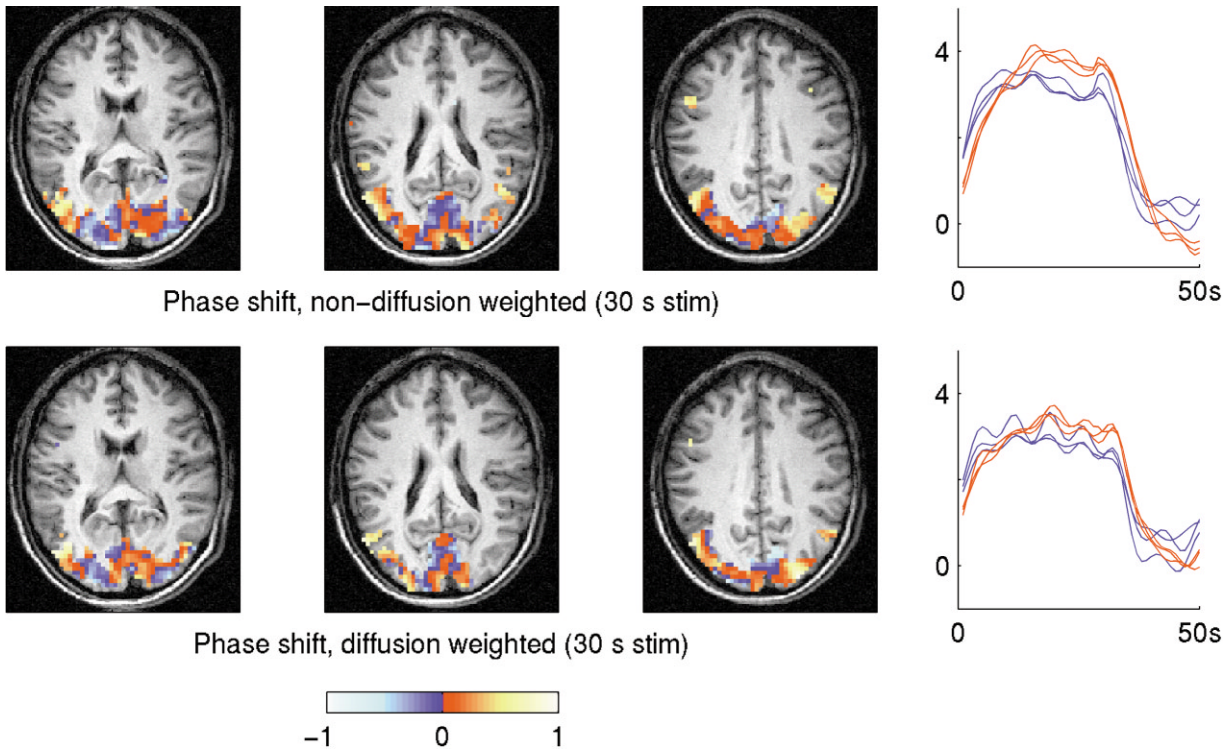

Figure 1. Several axial slices of an individual subject showing the estimated phase shift evoked by a periodic visual hemifield stimulation with a duration of 30 seconds and a control period of 30 seconds. The shown phase shifts were converted to time lags and were computed for brain regions that show at least a sample coherence of 0.8 (visual cortical areas). These time lags correspond to the trial averages computed for non-diffusion- and diffusion-weighted fMRI time series (right curves). The correlation between phase displacements of non-diffusion- (first row) and diffusion-weighted fMRI time series (second row) is above 0.8. This high correlation occurs for all subjects (see r_{ed} in Table 1) independently of the duration of stimulation.

The correlation between the percentage signal changes and the phase shifts depends on the duration of the visual stimulation (last two columns of Table 1). The correlation increases with decreasing length of visual stimulation. For visual stimuli of 30 seconds, the correlation is around zero (see first rows in Table 1, and Fig. 3). For the stimulation duration of 12 seconds, the correlation is around 0.4–0.5, and for the visual stimuli of 6 seconds the correlation is above 0.6 (see Table 1 and Fig. 4). Therefore, the shorter the duration of visual stimulation, the stronger the correlation between the percentage signal change and phase shift. This observation is obtained for both diffusion- and non-diffusion-weighted data sets for all subjects (Table 1). This fact can also be illustrated by looking at the high correlation between the phase maps of diffusion- and non-diffusion-weighted time courses.

DISCUSSION

In many brain studies, information about the temporal behavior of the hemodynamic response would be extremely interesting. In this work, the temporal dynamics of the BOLD response is investigated using varying durations of visual stimulation. Critical to the method is the estimation of the cross-covariance function and the spectral density matrix. The entries of this matrix can be used to compute estimations of further spectral parameters. In the present study, the spectral measures of coherence and phase shift were computed.

BOLD phase displacements between the cortical regions of individual subjects have also been discussed in the literature (6,7). Delays in peak times between different cortical regions in the order of seconds have been reported. However, the source of these phase shifts is still unknown. There are several possible explanations for this phenomenon. One interpretation is that the observed phase displacements may result from differences in the underlying vasculature (3,5). However, Rosen et al (6) noted the longest delays even in regions where the large vasculature is minimal. To further investigate this issue, we applied spectral methods to non-diffusion-and diffusion-weighted fMRI time series using visual stimuli of varying durations.

At 3 Tesla, the use of diffusion-weighting gradients removes most of the intravascular (but not the extravascular) signal contributions. The similar temporal behavior of the intra- and extravascular spaces, as indicated by similar spectral parameters for non-diffusion- and diffusion-weighted data, is not unexpected. Both are mainly determined by the concentration of deoxyhemoglobin in the blood, which changes instantaneously.

In the following, we discuss the observed stimulus-dependent distribution of activated voxels in the plane of phase shift and percentage signal change. In order to

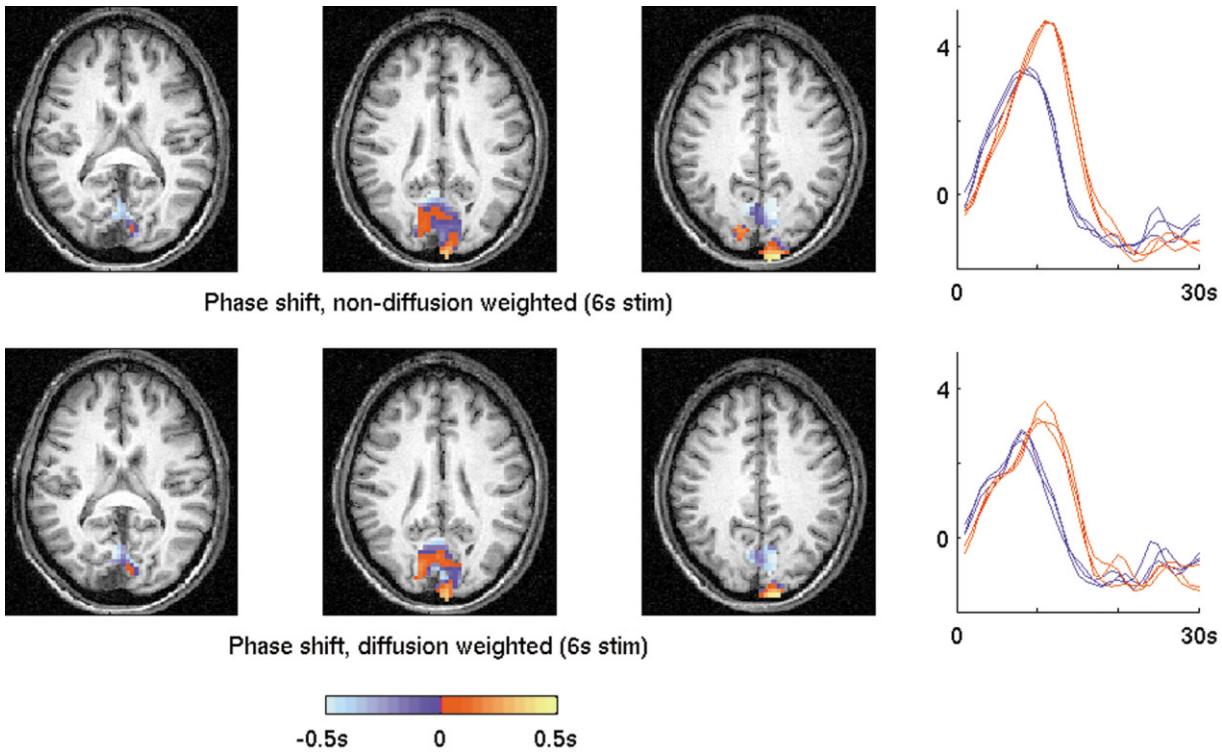

Figure 2. This illustration has the same content as Figure 1 for an individual subject using a visual stimulation of 6 seconds and a control period of 54 seconds. The trial averages (right curves) give first evidence for a relation between the phase shift and the percentage signal change. The phase shift increases with the signal change. The shorter the duration of visual stimulation, the stronger the correlation between the percentage signal change and the phase shift.

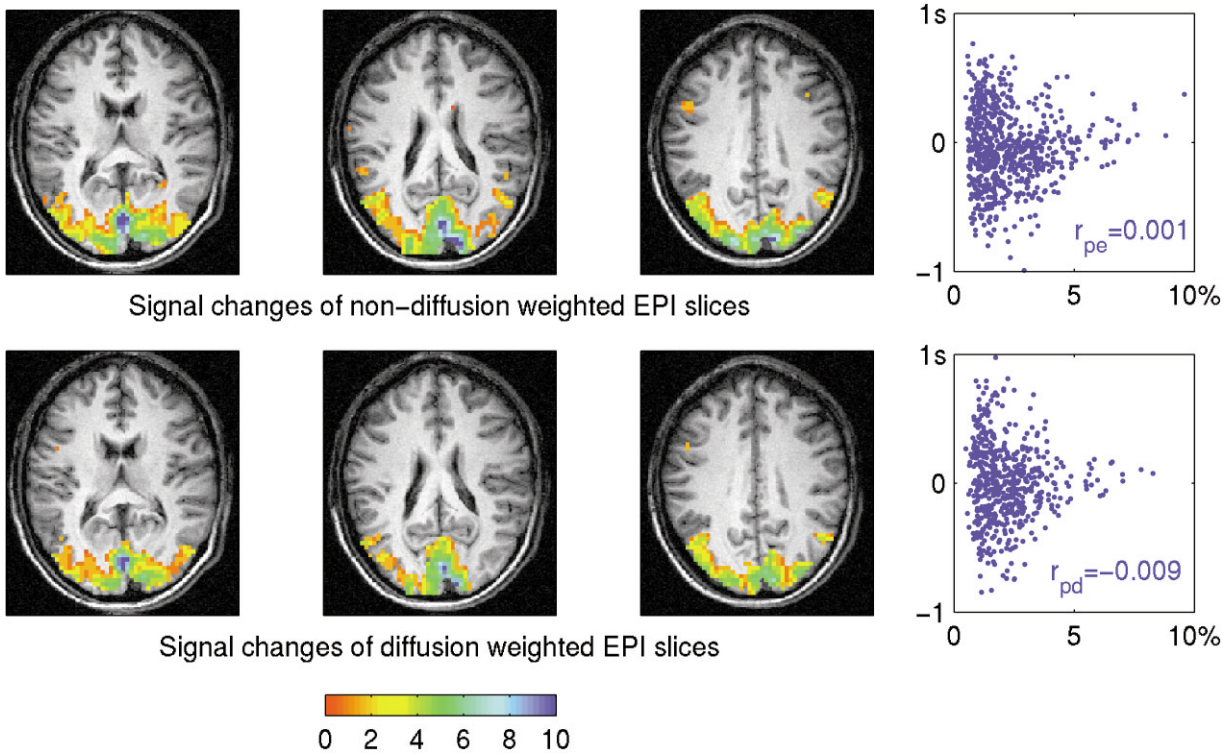

Figure 3. Maps of signal changes of non-diffusion- (first row) and diffusion-weighted fMRI time series (second row) evoked by a periodic visual stimulation with a duration of 30 seconds and a control period of 30 seconds. Percentage signal changes were computed for voxels that show a coherence above 0.8, i.e., voxels that are visualized in Figure 1. Therefore voxels with very low signal changes do not appear in the image. Correlation between signal changes and phase shifts are around zero for both non-diffusion-and diffusion-weighted data sets. For both subjects with 30-second stimulation, the correlation is around zero (see r_{pe} and r_{pd} in the first two columns of Table 1).

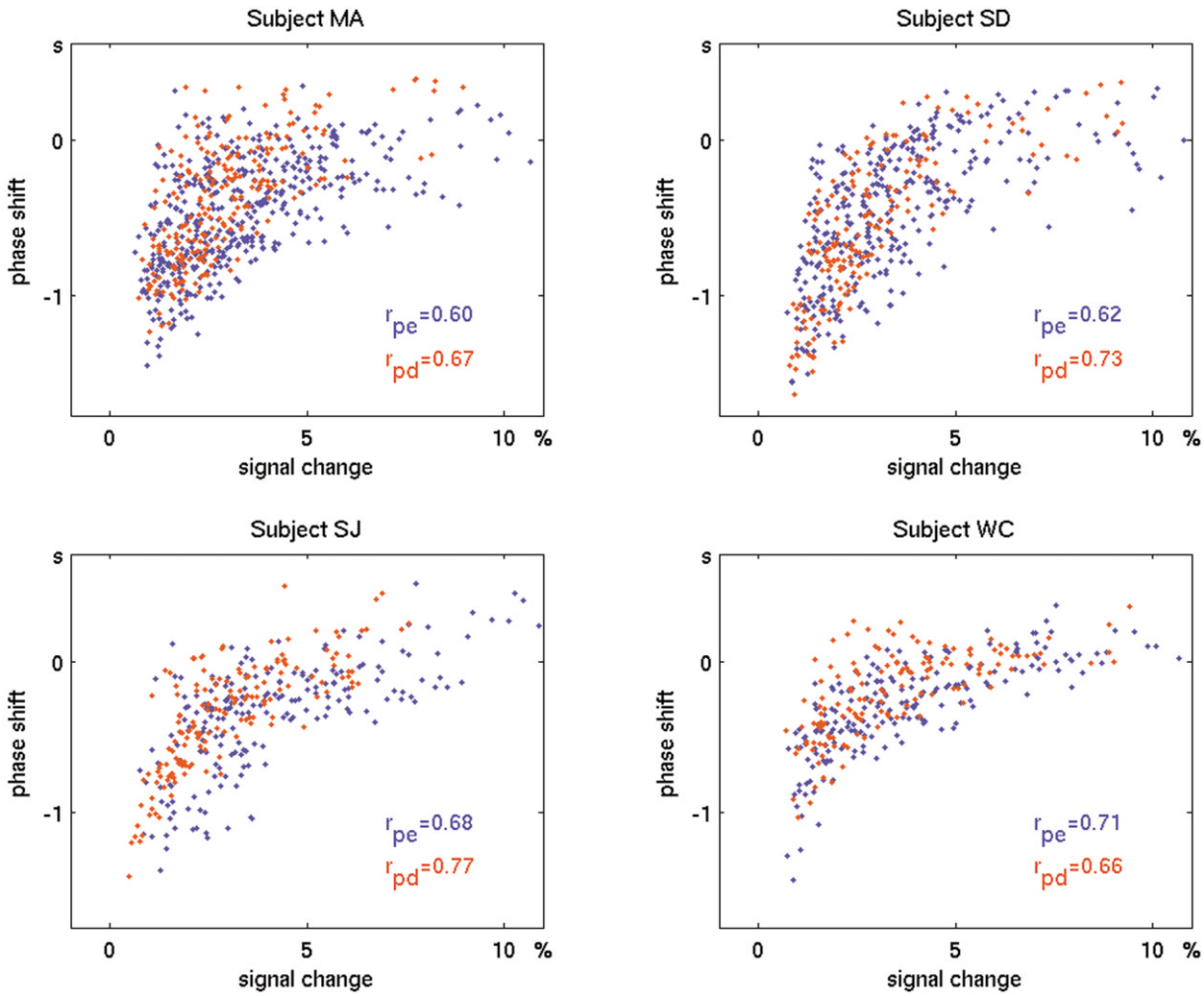

Figure 4. The correlation between percentage signal changes and phase shifts is above 0.6 for all subjects, with visual hemifield stimulation of 6 seconds (see Table 1 for confidence intervals of the correlation coefficients r_{pe} and r_{pd}). Voxels showing high signal changes also show a large phase shift to other voxels. Voxels showing an early response (large negative phase shift) show only very small signal changes. This behavior was observed for both non-diffusion- (blue dots) and diffusion-weighted data sets (red dots).

have a physically meaningful zero phase, we calibrated the phase shift to zero for the voxels with the highest signal change. For long visual stimuli, voxels with positive and negative phase shifts are present. In contrast, for shorter visual stimulation, voxels with a positive phase shift are nearly absent. This is not a side effect of calibrating the phase shift, because the zero phase shifts, i.e., the highest signal changes, are well located

Table 1
Correlation of BOLD Signal Changes and Phase Shifts*

Subject	t_s	M_N	r_{ed}	r_{pe}	r_{pd}
HS	30/30	30	0.81 (0.78,0.84) [510]	0.00 (–0.07,0.07) [688]	–0.01 (–0.09,0.08) [531]
SJ	30/30	30	0.80 (0.75,0.84) [259]	–0.07 (–0.17,0.03) [367]	0.02 (–0.09,0.14) [269]
KA	12/78	54	0.82 (0.77,0.85) [244]	0.44 (0.36,0.52) [397]	0.37 (0.26,0.47) [245]
PA	12/78	54	0.80 (0.73,0.85) [130]	0.52 (0.42,0.61) [237]	0.48 (0.34,0.60) [135]
MA	6/54	36	0.91 (0.89,0.93) [219]	0.60 (0.53,0.66) [429]	0.67 (0.59,0.74) [225]
SD	6/54	36	0.93 (0.91,0.95) [165]	0.62 (0.55,0.68) [342]	0.73 (0.65,0.79) [173]
SJ	6/54	36	0.89 (0.85,0.92) [151]	0.68 (0.60,0.75) [196]	0.77 (0.69,0.82) [161]
WC	6/54	36	0.85 (0.80,0.90) [119]	0.71 (0.64,0.78) [197]	0.66 (0.55,0.74) [140]

*Note: The correlation r_{ed} between phase shifts in non-diffusion- and diffusion-weighted fMRI time series is above 0.8 for all subjects, independently of the duration of the visual stimuli. For all correlation coefficients, confidence intervals are computed using a probability level of 0.05. The bracketed numbers show the number of coherent voxels in the map of phase shifts (see Fig. 1 and 2). The other two correlation coefficients r_{pe} and r_{pd} show the correlation between percentage signal changes and phase shifts for non-diffusion- and diffusion-weighted data sets. Both correlations r_{pe} and r_{pd} increase with decreasing length of visual stimulation. The column t_s shows the duration of stimulation and rest in seconds. The number M_N is the spectral window size that is used for computing the spectral density (see Eq. [7]).

in the primary visual areas for both the 6-second and the 30-second stimulus as demonstrated by the maps of phase shift.

In the case of the 6-second stimulus, the correlation between phase shift and percentage signal change means that the BOLD signal is higher at a later time. The higher the signal change, the larger the phase shift. One possible explanation for this surprising result is that larger vessels contribute to the higher signal changes. If this is the case, the observed correlation would be caused by the increased transit time of the blood. Evidence for a delay of the BOLD response of large draining veins with regard to that of the parenchyma has been found at a magnetic field of 1.5 Tesla (5).

An alternative explanation that involves the parenchyma could be a partial uncoupling of metabolism and flow right after the start of stimulation. Such effects could be brought on by the fast response (24,25), which could not be observed under our experimental conditions. As soon as the coupling between flow and metabolism is recovered, areas with higher oxygen consumption will respond with an increased blood flow. The higher content of deoxyhemoglobin at the beginning of the stimulus would induce a BOLD signal that appears later. However, determining the reasons behind this correlation requires further investigation. In the case of the long stimulus, voxels with a delayed BOLD response of lower amplitude (i.e., voxels with a positive phase shift) could be interpreted in terms of an additional activation in extrastriate visual areas.

Because of the nonlinearity of the BOLD response, the influence of the length of the stimulation to the phase-amplitude correlation could be nonlinear. To explore that possibility, further data are needed to quantity the dependence between the phase-amplitude correlation and the length of stimulation.

In conclusion, spectral methods were applied successfully to fMRI data obtained with varying durations of visual stimulation. The variation of the BOLD phase shifts was about 1 and 2 seconds for short and long stimuli, respectively. The experiments with short and long stimuli differed mainly in the distribution of the activated voxels in the plane of percentage signal change and phase shift. However, more work, including experiments with very short visual stimuli, is necessary to further investigate this effect.

REFERENCES

1. Marchini JL, Ripley BD. A new statistical approach to detecting significant activation in functional MRI. Neuroimage 2000;12:366–380.
2. Müller K, Lohmann G, Bosch V, von Cramon DY. On multivariate spectral analysis of fMRI time series. Neuroimage 2001;14:347–356.
3. Miezin FM, Maccotta L, Ollinger JM, Petersen SE, Buckner RL. Characterizing the hemodynamic response: effects of presentation rate, sampling procedure, and the possibility of ordering brain activity based on relative timing. Neuroimage 2000;11:735–759.
4. Menon RS, Luknowsky DC, Gati JS. Mental chronometry using latency-resolved functional MRI. Proc Natl Acad Sci U S A 1998;95:10902–10907.
5. Lee AT, Glover GH, Meyer CH. Discrimination of large venous vessels in time-course spiral blood-oxygen-level-dependent magnetic-resonance functional neuroimaging. Magn Reson Med 1995;33:745–754.
6. Rosen BR, Buckner RL, Dale AM. Event-related functional MRI: past, present, and future. Proc Natl Acad Sci U S A 1998;95:773–780.
7. Buckner RL, Koutstaal W, Schacter DL, Dale AM, Rotte M, Rosen BR. Functional-anatomic study of episodic retrieval. II. Selective averaging of event-related fMRI trials to test the retrieval success hypothesis. Neuroimage 1998;7:163–175.
8. Ogawa S, Menon RS, Tank DW, et al. Functional brain mapping by blood oxygenation level-dependent contrast magnetic resonance imaging. Biophys J 1993;64:800–812.
9. Weisskoff RM, Zuo CS, Boxerman JL, Rosen BR. Microscopic susceptibility variation and transverse relaxation: theory and experiment. Magn Reson Med 1994;31:601–610.
10. Song AW, Wong EC, Tan SG, Hyde JS. Diffusion weighted fMRI at 1.5 T. Magn Reson Med 1996;35:155–158.
11. Mildner T, Norris DG, Schwarzbauer C, Wiggins CJ. A qualitative test of the balloon model for BOLD-based MR signal changes at 3 Tesla. Magn Reson Med 2001;46:891– 899.
12. Hannan EJ. Multiple time series (In Russian). Moscow: Mir; 1974. 575 p.
13. Priestley MB. Spectral analysis and time series. London: Academic Press; 1981. 890 p.
14. Koopmans LH. The spectral analysis of time series. In: Birnbaum ZW, Lukacs E, editors. Probability and mathematical statistics. Vol. 22. London: Academic Press; 1974. 366 p.
15. Francis ST, Gowland PA, Bowtell RW. Continuous saturation EPI with diffusion weighting at 3.0T. NMR Biomed 1999;12:440–450.
16. Ugurbil K, Garwood M, Ellermann J, et al. Imaging at high magnetic fields: initial experiences at 4T. Magn Reson Q 1993;9:259–277.
17. Norris DG. Reduced power multi-slice MDEFT imaging. Magn Reson Imaging 2000;11:445– 451.
18. Friston KJ, Mechelli A, Turner R, Price CJ. Nonlinear responses in fMRI: the Balloon model, Volterra kernels, and other hemodynamics. Neuroimage 2000;12:466–477.
19. Lohmann G, Müller K, Bosch V, et al. LIPSIA—a new software system for the evaluation of functional magnetic resonance images of the human brain. Comput Med Imaging Graph 2001;25:449–457.
20. Press WH, Teukolsky SA, Vetterling WT, Flannery BP. Numerical recipes in C. Cambridge: Cambridge University Press; 1992. 994 p.
21. Winer B, Brown D, Michels K. Statistical principles in experimental design. New York: McGraw-Hill; 1991. 1057 p.
22. Friston KJ, Holmes AP, Worsley KJ, Poline JP, Frith CD, Frackowiak RSJ. Statistical parametric maps in functional imaging: a general linear approach. Hum Brain Mapp 1995;2:189–210.
23. Worsley KJ, Friston KJ. Analysis of fMRI time-series revisited—again. Neuroimage 1995;2:173–181.
24. Ernst T, Hennig J. Observation of a fast response in functional MR. Magn Reson Med 1994;32:146–149.
25. Hu X, Le TH, Ugurbil K. Evaluation of the early response in fMRI using short stimulus duration. Magn Reson Med 1997;37:877–884.